Applied Occupational and Environmental Hygiene

ISSN: 1047-322X (Print) 1521-0898 (Online) Journal homepage: https://www.tandfonline.com/loi/uaoh20

A Multi-Zone Model Evaluation of the Efficacy of Upper-Room Air Ultraviolet Germicidal Irradiation

Mark Nicas & Shelly L. Miller

To cite this article: Mark Nicas & Shelly L. Miller (1999) A Multi-Zone Model Evaluation of the Efficacy of Upper-Room Air Ultraviolet Germicidal Irradiation, Applied Occupational and Environmental Hygiene, 14:5, 317-328, DOI: 10.1080/104732299302909

To link to this article: https://doi.org/10.1080/104732299302909

Published online: 30 Nov 2010.

Applied Occupational and Environmental Hygiene
Volume 14: 317–328, 1999

1047-322X/99 $12.00 + .00

A Multi-Zone Model Evaluation of the Efficacy of Upper-Room Air Ultraviolet Germicidal Irradiation

Mark Nicas[1] and Shelly L. Miller[2]

[1]Center for Occupational and Environmental Health, School of Public Health, University of California, Berkeley, California, USA; [2]Department of Mechanical Engineering, University of Colorado, Boulder, Colorado, USA

Engineering controls can be used to reduce the spread of airborne infectious disease, particularly tuberculosis (TB), in high-risk settings. This article evaluates published data on the efficacy of upper-room air ultraviolet germicidal irradiation (UVGI). A three-zone representation of a TB patient room equipped with a germicidal UV lamp is developed. The lamp irradiates the upper-room zone and inactivates airborne mycobacteria; the unirradiated lower-room zone also contains a near-field zone surrounding the TB patient. Infectious particles are generated in the near-field zone and transported throughout the room by air flow between zones. Each zone is independently well-mixed; the whole room, however, is not well-mixed. The three-zone model is applied to a previously published study of UVGI against airborne mycobacteria in a test room. Based on the estimated slopes of the semi-log concentration decay curves for viable mycobacteria, and on the assumption that the test room was essentially well-mixed, the published study reported that UVGI provided 10 to 25 equivalent air changes per hour. However, when the same decay curve slopes are interpreted in the context of the three-zone model, UVGI is seen to be far less effective in reducing exposure intensity near the TB patient. Near-field exposure intensity is relevant because health care workers are usually in close proximity to the TB patients they attend. In general, the interpretation of concentration decay data depends on the specific model of room air mixing that is assumed appropriate. It is recommended that tests of the efficacy of UVGI and other control devices against airborne microorganisms be based on steady-state concentration measurements rather than concentration decay measurements, because the former measurements do not require inferences based on a particular model.

Keywords Tuberculosis, Ultraviolet Germicidal Radiation, Multi-Zone Modeling

Many infectious diseases are spread through the air, including viral diseases such as measles and bacterial diseases such as tuberculosis (TB). TB has recently reemerged as a serious public and occupational health problem,[1–5] although there is evidence that TB incidence may have stabilized in some U.S. cities.[6,7] Infection can occur when a susceptible person inhales as few as one respirable particle (termed a *droplet nucleus*) carrying viable *Mycobacterium tuberculosis* (*M. tb*).[8] Persons who become infected with *M. tb* and who do not undergo antibiotic prophylaxis have a 10 percent lifetime risk of developing active disease.[9,10] Given the increased incidence of multi-drug-resistant TB, which is associated with increased morbidity and mortality, primary prevention of disease transmission has assumed greater importance.[10–12]

To control TB transmission, strategies that reduce the generation and transport of *M. tb* aerosol, as well as programs that identify and treat infectious individuals, need to be implemented. For TB patient isolation rooms, the Centers for Disease Control and Prevention (CDC) recommend a ventilation rate of at least six air changes per hour (ACH, h^{-1}),[10] of which at least two are outside air.[13,14] Isolation room exhaust air must be either directed outside the building or passed through a high-efficiency particulate air filter prior to recirculation. The isolation room should be under negative pressure relative to adjacent areas. The CDC also recommends that, where feasible, the air-exchange rate be increased to ≥ 12 ACH by modifying the ventilation system or by using auxiliary means. Many isolation rooms currently receive less than 6 ACH,[15] and renovating facilities to achieve rates of 6–12 ACH can be expensive. Thus, there is interest in auxiliary means to remove viable *M. tb* from room air; these include the use of upper-room air ultraviolet germicidal irradiation (UVGI).

Commercially available germicidal lamps are low-pressure mercury vapor lamps emitting an almost monochromatic radiation of wavelength 254 nm.[14] The optimal wavelength for inactivating microorganisms ranges from 250–270 nm, depending on the microorganism.[15] For TB control, UVGI is used in two configurations: ventilation duct irradiation and upper-room

air irradiation.[14] For upper-room air irradiation, the lamps are suspended from the ceiling or attached to the walls; the bottom of the lamp is usually shielded to direct radiation in the horizontal and upward directions. The objective of this configuration is to inactivate *M. tb* in the upper part of the room while minimizing radiation exposure to persons in the lower part of the room. If the room is relatively well-mixed, inactivation of *M. tb* in the upper zone effectively reduces the viable *M. tb* concentration in the lower zone.

The first observation of the efficacy of upper-room air UVGI to control airborne infection was by Wells in 1934.[16] Since that time there has been little systematic investigation of UVGI, and the few studies conducted in full-sized rooms have shown that efficacy varies widely. One study reported that upper-room air UVGI achieved substantial inactivation of mycobacteria in the range of 10 to 25 equivalent ACH depending on the total power of the UV lamps.[17] This study is described in more detail subsequently. Another study conducted in a hospital waiting room found that upper-room air UVGI reduced the concentration of airborne colony-forming units by only 14–19 percent.[18,19]

Anecdotal evidence also suggests that UVGI is effective. For example, Stead and colleagues investigated an incident in which 159 employees were exposed for an 84-day period to a patient who had cavitary TB and persistently positive sputum smears.[20] There were no documented conversions of tuberculin skin tests. The authors attributed this favorable experience to the use of UVGI. The isolation rooms at this hospital, however, were provided with ventilation of 15 ACH and the operating room where the patient underwent a lobectomy had 48 ACH.

In this article we examine the efficacy of upper-room air UVGI for controlling TB transmission in rooms that may not be well-mixed. We describe two alternative multi-zone models. We then apply a three-zone model to evaluate published data from a study in which aerosolized *M. bovis* were exposed to upper-room air UVGI, and the decay in the viable *M. bovis* concentration was subsequently measured.[17] We demonstrate that for an imperfectly mixed room, the traditional interpretation of concentration decay data can lead to overestimating the effective contaminant removal rate and underestimating the steady-state concentration in the near field of the emission source. Near-field exposure intensity is especially relevant because health care workers are usually in close proximity to the TB patients they attend. Therefore, the published viable *M. bovis* concentration decay data could easily have been misinterpreted to overestimate UVGI efficacy.

MULTI-ZONE MODELS

The Two-Zone Model

A TB patient room is conceptually divided into an upper and lower zone (Figure 1).[21] Air within each zone is presumed perfectly mixed, but the air flow between the two zones is limited. The air-exchange rate between the upper and lower zone is denoted β; the upper and lower zone volumes are denoted V_U and V_L. The UV lamp irradiates and inactivates only the airborne *M. tb* in the upper zone. The TB patient (the emission source) is located in the lower zone.

The exact form of the solution equations for this model depend on the zones in which the supply and exhaust points for mechanically supplied air (HVAC system) and infiltration air (doors and windows) are located. In Figure 1, all air enters and exits the room via the lower zone, but locations of air entry and exit points will differ from room to room. The solution equations describing the *M. tb* aerosol concentration (#/m^3) in the upper and lower zones, C_U and C_L, as a function of time have the following general forms:

$$C_U(t) = \delta_1 \cdot e^{\lambda_1 \cdot t} + \delta_2 \cdot e^{\lambda_2 \cdot t} + \delta_3 \quad [1]$$

$$C_L(t) = \delta_4 \cdot e^{\lambda_1 \cdot t} + \delta_5 \cdot e^{\lambda_2 \cdot t} + \delta_6 \quad [2]$$

The parameters λ_1 and λ_2 (min^{-1}) depend on the values of: (*i*) the zone volumes V_U and V_L (m^3); (*ii*) the room air supply/exhaust rate, Q (m^3/ min); (*iii*) the interzonal air-exchange rate, β (m^3/ min); (*iv*) the natural die-off rate constant for *M. tb* in air, k_1 (min^{-1}); and (*v*) the UV-induced inactivation rate constant for *M. tb* in air, k_2 (min^{-1}). The values of the coefficients δ_1 through δ_6 depend on the same parameters, as well as the viable *M. tb* emission rate, G (#/ min), and the initial mycobacteria concentrations in the upper and lower zones, $C_{U,0}$ and $C_{L,0}$. In realistic scenarios, the parameters λ_1 and λ_2 will be real, distinct, negative numbers. Therefore, as t gets large, the terms $e^{\lambda_1 \cdot t}$ and $e^{\lambda_2 \cdot t}$ go to zero, and the steady-state concentrations in the upper and lower zones, $C_{U,SS}$ and $C_{L,SS}$, equal the parameters δ_3 and δ_6, respectively.

Proponents of upper-room air UVGI believe that the interzonal air-exchange rate is substantial in most rooms,[22] in which case β is substantially greater than Q. Given this condition, the two-zone model usually predicts that $C_{L,SS} \cong C_{U,SS}$. In other words, the room behaves as if it were perfectly mixed, even though it has two distinct zones. The strategic advantage of such behavior is that if UVGI has a substantial *M. tb* inactivation rate k_2, then UVGI applied to the upper zone effectively reduces the viable *M. tb* concentration throughout the lower zone.

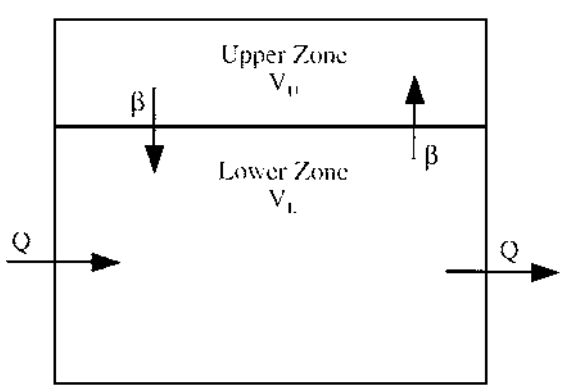

FIGURE 1

A schematic representation of a two-zone room. V_U and V_L are the upper zone and lower zone volumes (m^3). Q is the total room supply/exhaust air rate (m^3/ min), with all air supply and exit points in the lower zone. β is the interzonal air-exchange rate (m^3/ min).

Once emission ceases (G = 0), equations of the same form as (1) and (2) describe the *M. tb* aerosol concentration in the two zones, except that the coefficients δ_3 and δ_6 equal zero; also, the four remaining δ coefficient values differ from the case when G > 0. The values of the parameters λ_1 and λ_2 remain the same because they do not depend on the emission rate or the initial *M. tb* concentrations in the different zones.

The Three-Zone Model

An alternative, physically plausible model for a TB patient room equipped with upper-room air UVGI is a three-zone model. The room is conceptually divided into an upper zone and a lower zone, but a near-field zone located within the lower zone contains the patient (Figure 2).[23–25] Air within each zone is presumed perfectly mixed, but the air exchange between the upper and lower zones, and between the lower and near-field zones, is limited. The upper/lower zone air-exchange rate is denoted β_1, and the lower/near-field zone air-exchange rate is denoted β_2. The volume of the near-field zone is denoted V_{NF}. The UV lamp irradiates only the airborne *M. tb* in the upper zone.

The exact solution equations depend on the zones in which the supply and exhaust points for mechanically supplied air (the HVAC system) and infiltration air (doors and windows) are located. In Figure 2, all air enters and exits the room via the lower zone, although this need not be the case. The general equations for the *M. tb* aerosol concentration as a function of time in the upper, lower, and near-field zones are as follows:

$$C_U(t) = \omega_1 \cdot e^{\lambda_1 \cdot t} + \omega_2 \cdot e^{\lambda_2 \cdot t} + \omega_3 \cdot e^{\lambda_3 \cdot t} + \omega_4 \quad [3]$$

$$C_L(t) = \omega_5 \cdot e^{\lambda_1 \cdot t} + \omega_6 \cdot e^{\lambda_2 \cdot t} + \omega_7 \cdot e^{\lambda_3 \cdot t} + \omega_8 \quad [4]$$

$$C_{NF}(t) = \omega_9 \cdot e^{\lambda_1 \cdot t} + \omega_{10} \cdot e^{\lambda_2 \cdot t} + \omega_{11} \cdot e^{\lambda_3 \cdot t} + \omega_{12} \quad [5]$$

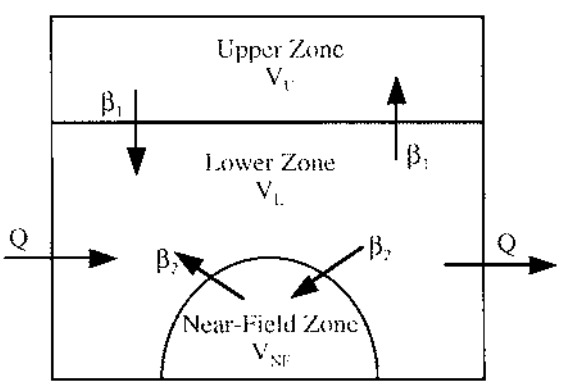

FIGURE 2
A schematic representation of a three-zone room. V_U, V_L, and V_{NF} are the respective upper zone, lower zone, and near-field zone volumes (m^3). Q is the total room supply/exhaust air rate (m^3/ min), with all air supply and exit points in the lower zone. β_1 is the air-exchange rate between the upper and lower zones (m^3/ min). β_2 is the air-exchange rate between the lower and near-field zones (m^3/ min).

The λ values depend on the zone volumes (V_U, V_L, V_{NF}), the ventilation characteristics of the room (β_1, β_2, Q), and the inactivation rate constants (k_1 and k_2). The values of the ω coefficients depend on these same parameters, as well the *M. tb* emission rate and the initial *M. tb* concentrations in the three zones. In realistic scenarios, λ_1, λ_2, and λ_3 will be real, distinct, negative numbers. Therefore, as *t* gets large, the terms $e^{\lambda_1 \cdot t}$, $e^{\lambda_2 \cdot t}$, and $e^{\lambda_3 \cdot t}$ go to zero, and the steady-state *M. tb* concentrations $C_{U,SS}$, $C_{L,SS}$, and $C_{NF,SS}$ are equal to the respective coefficients ω_4, ω_8, and ω_{12}.

It happens that $C_{NF,SS}$ is strongly influenced by the term G/β_2. This influence is evident in the following approximation:

$$C_{NF,SS} \cong \frac{(k_2 \cdot V_U + \beta_1)}{[k_2 \cdot V_U(\beta_1 + Q) + \beta_1 \cdot Q]} \cdot G + \frac{G}{\beta_2} \quad [6]$$

Equation 6 assumes that $k_1 \ll k_2$, which is reasonable for *M. tb* as will be discussed. The equation also assumes that all air supply and exit points are in the lower zone, a situation which likely pertained in a test room study that will also be described. If β_2 is relatively small compared to the upper/lower zone air-exchange rate β_1, the room will not behave as if it were well-mixed, and the strategic advantage of upper-room air UVGI will be diminished. One consequence is that the *M. tb* aerosol concentration near the patient will be significantly greater than elsewhere in the lower portion of the room.

For comparison with $C_{NF,SS}$, Equation 7 describes the steady-state *M. tb* concentration in a well-mixed (single-zone) room, denoted $C_{WM,SS}$, with an equivalent air supply rate denoted Q_E:[23]

$$C_{WM,SS} = \frac{G}{Q_E} \quad [7]$$

Once *M. tb* emission ceases (G = 0), equations of the same form as (3)–(5) describe the decay in aerosol concentration in the three zones, except that the coefficients ω_4, ω_8, and ω_{12} equal zero, and the values of the other ω coefficients differ from the case when G > 0. As with the two-zone model, the values of the parameters λ_1, λ_2, and λ_3 do not depend on the *M. tb* emission rate or initial concentrations in the different zones.

The three-zone model is now applied to a study by Riley, Knight, and Middlebrook which investigated the efficacy of upper-room air UVGI against aerosolized *M. bovis* bacteria.[17] This study, which is more than 20 years old, still provides the best experimental data on the use of UVGI against airborne mycobacteria in a real-world setting.

THE *M. bovis* ROOM STUDY

The Three-Zone Model of the Test Room

Riley and colleagues released viable *M. bovis* BCG aerosol into a test room, and created a presumably uniform room concentration by using a fan to mix up the room air. Once aerosol release ceased, they measured the concentration decay of viable *M. bovis*, with and without upper-room air UVGI, at a sampling

point 0.8 m (32 in) off the floor near the center of the room. As described, the total room volume was 64 m^3 (2260 ft^3), with floor dimensions of 18.4 m^2 (198 ft^2) and a ceiling height of 3.5 m (11 ft 5 in).

On the first test day, one 17-watt (W) lamp was operated with the UV tubes facing the ceiling and baffled to prevent radiation below the edges of the lamp fixture. In this configuration, the irradiated upper-room zone nominally extended down 0.61 m (2 ft) from the ceiling, so the theoretical upper zone volume V_U was 11.2 m^3 (396 ft^3). On the second and third test days, a 29-W lamp was operated, in addition to the 17-W lamp. This 29-W lamp was operated with the UV tubes facing the floor and baffled to control the downward inclination of radiation. For the second and third test days, the irradiated upper zone nominally extended down approximately 1.65 m (5 ft 5 in) from the ceiling; the theoretical upper zone volume V_U was 30.4 m^3 (1073 ft^3). No mechanical ventilation was operating in the room during the experiments, and the door to the room was sealed. However, air infiltration/exfiltration was possible through one (or more) windows which presumably were located in the room's lower zone. Note that a room diagram was not provided, and measurements of air flows, air speeds, air temperature, humidity, and UV radiation intensity were not taken.

Consider a hemispherical near-field zone 1 m (3.3 ft) in radius around the *M. bovis* aerosol generator; the latter was likely placed on a table or the room floor (Figure 2). The hemisphere geometry also represents the potential near-field zone around a TB patient lying on a bed, and 1 m approximates the distance between a health care worker and the patient. The near-field zone volume V_{NF} is 2.1 m^3 (i.e., $\frac{2}{3}\pi r^3$), in which case the remaining lower zone volume V_L is 50.7 m^3 for the first test day, and 31.5 m^3 for the second and third test days.

To assign interzonal air exchange values, assume that the average random air speed in the test room was 3 m/min (10 fpm), which represents relatively still air.[27] In a multi-zone model, it is assumed that air moves into a given zone through half the interzonal surface area, and moves out of the zone through the other half. Therefore: $\beta_1 = 9.2\ m^2 \times 3 m/min = 28\ m^3/min$ (990 cfm), and $\beta_2 = 3.1\ m^2 \times 3\ m/min = 9.6\ m^3/min$ (340 cfm). In the β_2 calculation, it is assumed that the base of the hemisphere lies on a physical surface (table, floor, or bed), in which case its surface area is not available for air flow. Therefore, β_2 is the product of the average air speed and half the surface area of a hemisphere (πr^2). For the assumed upper and near-field zone volumes, the magnitudes of β_1 and β_2 are substantial with respect to the number of air exchanges per unit time. That is, β_1/V_U ranges from 0.94 min^{-1} (second and third test days) to 2.5 min^{-1} (first test day), and β_2/V_{NF} is 4.6 min^{-1}.

The three-zone model is formulated from a material balance applied to the number of viable *M. bovis* in each zone of the room. The following set of differential equations describes the rate of change of the viable *M. bovis* concentration with time in the respective upper, lower, and near-field zones, with ongoing emission at constant rate G into the near-field zone:

$$\frac{dC_U}{dt} = \frac{\beta_1}{V_U} \cdot C_L(t) - \frac{[(k_1 + k_2) \cdot V_U + \beta_1]}{V_U} \cdot C_U(t) \quad [8]$$

$$\frac{dC_L}{dt} = \frac{\beta_2}{V_L} \cdot C_{NF}(t) + \frac{\beta_1}{V_L} \cdot C_U(t) - \frac{(k_1 \cdot V_L + \beta_1 + \beta_2 + Q)}{V_L} \cdot C_L(t) \quad [9]$$

$$\frac{dC_{NF}}{dt} = \frac{G}{V_{NF}} + \frac{\beta_2}{V_{NF}} \cdot C_L(t) - \frac{(k_1 \cdot V_{NF} + \beta_2)}{V_{NF}} C_{NF}(t) \quad [10]$$

In the above equations, k_1 is the rate constant for the natural die-off of *M. bovis* in air and k_2 is the rate constant for the UV-induced inactivation of *M. bovis*. Based on data for *M. tb* summarized by Hopewell,[26] it is estimated that $k_1 = .00235\ min^{-1}$. Given Equations 8–10, Appendix 1 presents general expressions for the rate constants λ_1, λ_2, and λ_3, and for the coefficients ω_1 through ω_{12}, that apply to the general solutions in Equations 3–5.

Reported Data and Inference

Table I summarizes the data reported for the three test days.[17] The slopes of the observed semi-log concentration decay curves were given in terms of equivalent room air changes per hour (Eq ACH). Consider the first test day. The reported slopes were 2 Eq ACH with UV lights off, and 12 Eq ACH with one 17-W UV light on. Based on this difference, Riley et al. inferred

TABLE I
Three-Zone model Parameters for the *M. bovis* UVGI room study

	Day 1[A]	Day 2[B]	Day 3[B]
Reported Eq ACH, UV off	2	2.5[C]	4
Reported Eq ACH, UV on	12	21	37
Required k_2 value (min^{-1})	1.28	0.80	1.95
$C_{WM,SS}$ (#/m^3) with UV on based on reported Eq ACH	G/12.8	G/22.5	G/39.5
$C_{NF,SS}$ (#/m^3) with UV on based on reported Eq ACH	G/5.3	G/6.0	G/6.8
$C_{NF,SS}/C_{WM,SS}$	2.4	3.8	5.8
$C_{L,SS}$ (#/m^3) with UV on based on reported Eq ACH	G/11.6	G/15.7	G/23.4
$C_{U,SS}$ (#/m^3) with UV on based on reported Eq ACH	G/17.6	G/29.4	G/72.9
$C_{NF,SS}/C_{U,SS}$	3.3	4.9	10.7

[A] One 17-W UV light fixture was operated on the first test day.
[B] One 17-W and one 29-W UV light fixture (supplying a total of 46 W) were operated on the second and third test days.
[C] The Eq ACH with UV lights off was reported as an estimate of 2 to 3 Eq ACH. The midpoint value of 2.5 Eq ACH was chosen for this analysis.

that UVGI with one 17-W fixture added 10 Eq ACH. Given a perfectly mixed room volume of 64 m^3, 12 Eq ACH represents $Q_E = 12.8\ m^3/min$, and given that bacilli are emitted at constant rate G, the steady-state concentration at all points in the room, $C_{WM,SS}$, would equal G/12.8 according to Equation 7.

Based on the three-zone model with the previously posited parameter values for the first test day ($V_U = 11.2\ m^3$, $V_L = 50.7\ m^3$, $V_{NF} = 2.1\ m^3$, $\beta_1 = 28\ m^3/min$, $\beta_2 = 9.6\ m^3/min$, $k_1 = .00235\ min^{-1}$), and with $Q = 2\ m^3/min$ (which produces an observed slope of 2 Eq ACH with UV lights off), an observed slope of 12 Eq ACH with UV lights on requires that $k_2 = 1.28\ min^{-1}$. Table I lists the k_2 values for the three test days required to reproduce the reported Eq ACH values with UV lights on. As will be explained, k_2 was computed using an iterative procedure. As will also be described, the computed k_2 value depends on the posited average random air speed, but is similar whether one assumes a two-zone or three-zone model.

For the posited room conditions pertaining on the first test day with $k_2 = 1.28\ min^{-1}$ (which produces the observed slope of 12 Eq ACH), the three-zone model predicts the near-field steady-state concentration to be G/5.3, which is 2.4-fold greater than the estimate $C_{WM,SS} = G/12.8$ for the same test day based on the well-mixed room assumption. That is, if a room is not well mixed, $C_{WM,SS}$ underestimates the steady-state bacilli concentration near the source. For the three test days under analysis, the ratio $C_{NF,SS}/C_{WM,SS}$ ranges from 2.4–5.8 (see Table I). Again, the three-zone model predicts higher concentrations near the source than would be predicted using the Riley et al. decay curve slopes and the well-mixed room assumption. Limited air flow between zones also signifies that the steady-state bacilli concentrations will differ by room location. For example, again consider the first test day. Given the previously posited parameter values with UV lights on, the three-zone model predicts that: $C_{NF,SS} = G/5.3$, $C_{L,SS} = G/11.6$, and $C_{U,SS} = G/17.6$. This 3.3-fold range in concentrations reflects a room that is, of course, not well-mixed.

The following question arises: Shouldn't the lower effective ventilation rate in the near-field zone be reflected in the slope of the semi-log decay curve at this same position? For example, on the first test day, shouldn't the observed slope in the near-field zone be considerably less than 12 Eq ACH? The answer is, not necessarily.

Consider the set of three-zone model decay equations corresponding to the first test day with UV lights on, but starting from an initial uniform room concentration of 100 per m^3 (this concentration is a convenient value that does not correspond to the actual *M. bovis* concentrations). For the parameter values discussed previously, Figure 3 shows the predicted semi-log decay curves in the three zones. Although the initial portions of these curves are nonlinear, they are transient and easy to miss. After a short time, all three curves appear as straight lines with the same slope. The value of this slope corresponds to the least negative λ parameter (termed the dominant λ parameter) in Equations 3–5.[23,28] If by convention, $|\lambda_1| < |\lambda_2| < |\lambda_3|$, then for

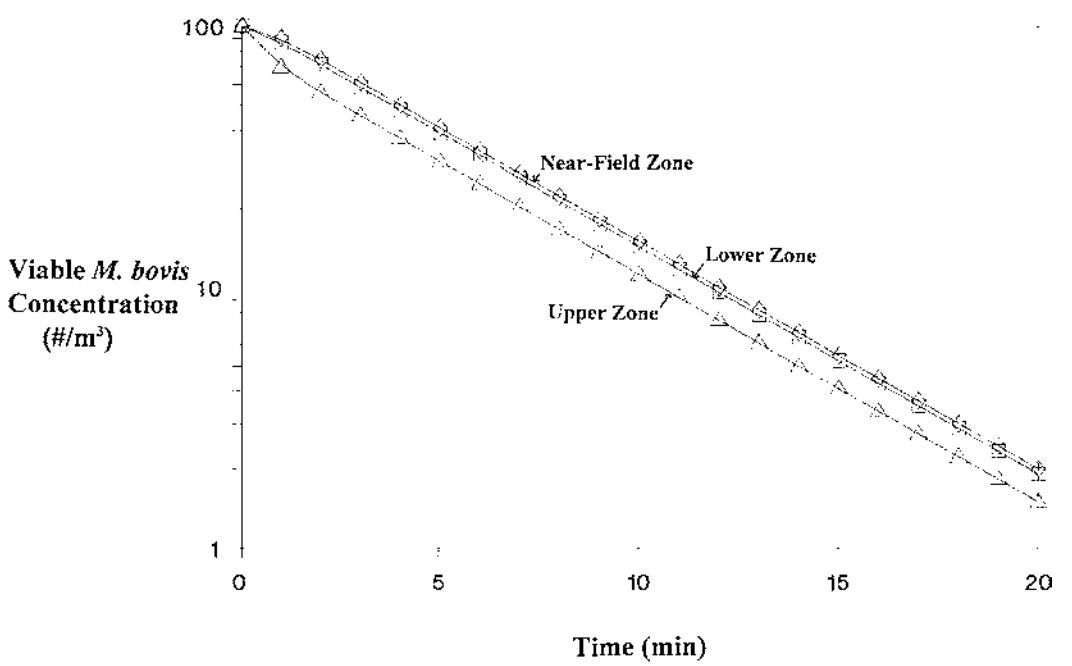

FIGURE 3

The decay in the viable *M. bovis* concentration according to the three-zone model, where the initial concentration is 100 per m^3 in all three zones. Model parameter values are as follows: $V_U = 11.2\ m^3$, $V_L = 50.7\ m^3$, $V_{NF} = 2.1\ m^3$, $Q = 2\ m^3/min$, $\beta_1 = 28\ m^3/min$, $\beta_2 = 9.6\ m^3/min$, $k_1 = .00235\ min^{-1}$, $k_2 = 1.28\ min^{-1}$.

the three zone-model parameter values posited for test day one, $\lambda_1 = -0.20\ min^{-1}$, $\lambda_2 = -4.06\ min^{-1}$, and $\lambda_3 = -4.87\ min^{-1}$. The actual decay equations are as follows:

$$C_U(t) = 72.5 \cdot e^{-0.20 \cdot t} + 24.9 \cdot e^{-4.06 \cdot t} + 2.6 \cdot e^{-4.87 \cdot t} \quad [11]$$

$$C_L(t) = 103.9 \cdot e^{-0.20 \cdot t} - 2.8 \cdot e^{-4.06 \cdot t} - 1.1 \cdot e^{-4.87 \cdot t} \quad [12]$$

$$C_{NF}(t) = 108.6 \cdot e^{-0.20 \cdot t} - 25.2 \cdot e^{-4.06 \cdot t} + 16.6 \cdot e^{-4.87 \cdot t} \quad [13]$$

In the above equations, the exponential terms involving λ_2 and λ_3 effectively disappear after two minutes, in which case all three trajectories appear as simple exponential decays governed by the dominant rate constant, $\lambda_1 = -0.20\ min^{-1}$ (= 12 Eq ACH).

The UV-Induced Inactivation Rate Constant

The k_2 values in Table I were computed in the context of the three-zone model as follows. Consider the reported decay slopes for the first test day of 2 Eq ACH with UV lights off, and 12 Eq ACH with UV lights on. Given the set of parameter values previously described, setting $Q = 2.0\ m^3/min$ with UV lights off ($k_2 = 0$) reproduced the reported slope of 2 Eq ACH. Alternative k_2 values were then inserted into the expression for λ_1 (see Appendix 1) until $\lambda_1 = -0.20\ min^{-1}$ (= 12 Eq ACH) was obtained.

The curve labeled "3 m/min" in Figure 4 shows how the Eq ACH value varies with k_2. By inspection, 12 Eq ACH corresponds to $k_2 = 1.28\ min^{-1}$. Figure 4 depicts two other curves generated in a similar manner except that the assumed average random air speeds were 1.5 m/min (5 fpm) and 15 m/min (50 fpm). For these latter air speeds, 12 Eq ACH corresponds to $k_2 = 2.12\ min^{-1}$ and $k_2 = 1.00\ min^{-1}$, respectively. The differences between the three curves demonstrate that the posited average random air speed affects the k_2 value inferred from the reported decay slope; the required k_2 value decreases as the average air speed increases. This result is intuitively reasonable. The parameter λ_1 depends on the interzonal air flows β_1 and β_2, which in turn depend on the average random air speed. As the air speed increases, the effect of UVGI in the upper zone is more rapidly transferred throughout the room. Given that λ_1 represents a clearance rate, a higher air speed value requires a lower k_2 value to achieve the same fixed rate of clearance. However, k_2 is expected to approach a limiting value as the air speed becomes large and the room becomes perfectly mixed.

For air speeds of 1.5, 3, 7.5, and 15 m/min, Table II lists the three-zone model k_2 values required to reproduce the reported decay slopes for each test day with UV lights on. Table II also lists the k_2 values computed in the context of the two-zone model that reproduce the reported slopes. For the two-zone model, it was assumed that $k_1 = .00235\ min^{-1}$, $V_U = 11.2\ m^3$, and $V_L = 52.8\ m^3$ on test day one, and $V_U = 30.4\ m^3$ and $V_L = 33.6\ m^3$ on test days two and three. The value of β depends directly on the average random air speed. Table II shows there is

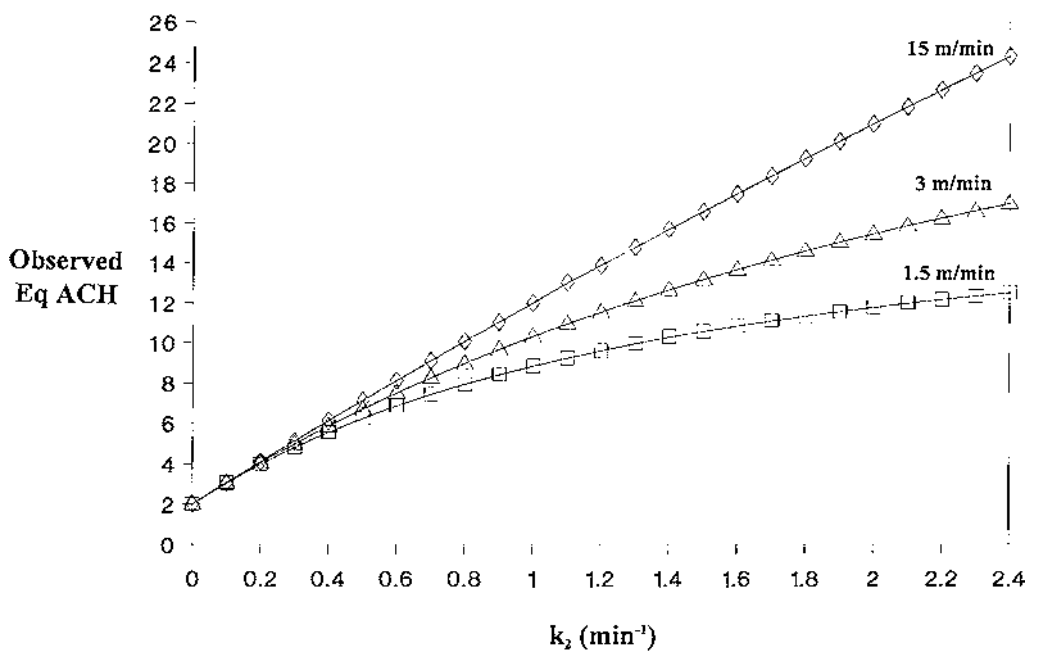

FIGURE 4

The observed number of equivalent air changes per hour as a function of the UV-induced *M. bovis* inactivation rate constant k_2 (min^{-1}) according to the three-zone model. The relationship is shown for average random air speeds (m/min) of 1.5, 3, and 15. Other model parameter values are as follows: $V_U = 11.2\ m^3$, $V_L = 50.7\ m^3$, $V_{NF} = 2.1\ m^3$, $Q = 2\ m^3/min$, $k_1 = .00235\ min^{-1}$. The values of β_1 and β_2 vary with the average random air speed.

TABLE II

UV-Induced inactivation rate constants k_2 required to reproduce the reported viable *M. bovis* concentration decay curve slopes[A]

Test day	Model	1.5 m/min	3 m/min	7.5 m/min	15 m/min
Day #1, 12 Eq ACH	Two-Zone	2.10	1.28	1.06	1.00
with UV on[B]	Three-Zone	2.12	1.28	1.06	1.00
Day #2, 21 Eq ACH	Two-Zone	1.19	0.79	0.69	0.67
with UV on[C]	Three-Zone	1.22	0.80	0.69	0.67
Day #3, 37 Eq ACH	Two-Zone	—[E]	1.91	1.32	1.23
with UV on[D]	Three-Zone	—[E]	1.95	1.33	1.23

[A]The k_2 values are computed for both the two-zone and three-zone models. The assumed values of the other model parameters are described in the text.

[B]One 17-W UV light fixture was operated. With UV lights off, the reported decay curve slope was 2 Eq ACH.

[C]One 17-W and one 29-W UV light fixture were operated. With UV lights off, the reported decay curve slope was estimated as 2 to 3 Eq ACH; the midpoint value of 2.5 Eq ACH was used for this analysis.

[D]One 17-W and one 29-W UV light fixture were operated. With UV lights off, the reported decay curve slope was 4 Eq ACH.

[E]No value of k_2 could be found that reproduced the reported decay curve slope of 37 Eq ACH.

little difference between the k_2 values based on these alternative multi-zone models.

In the same paper reporting the *M. bovis* test room data, Riley et al. summarized laboratory data on the UV susceptibility of different organisms.[17] Airborne *M. bovis* were subjected to UV doses of 126 or 510 $\mu W \cdot sec/cm^2$ over a 6-second period in a specially designed apparatus. Efficacy was expressed in terms of a metric Z:

$$Z = \frac{\ln(N_0/N_{UV})}{\text{Dose in } \mu W \cdot sec/cm^2}$$

where N_0 is the viable colony count without UV exposure, and N_{UV} is the viable colony count after receiving the UV dose. For two different cultures of *M. bovis*, Riley et al. reported Z values averaging .0025 and .0037; the specific dose associated with each value was not specified. Based on a total of 26 tests, the overall average Z value for *M. bovis* was 0.0031.

It can be shown that the inactivation rate constant k_2 is equal to the product $Z \cdot I$, where I is intensity ($\mu W/cm^2$) and k_2 is based on the time unit sec^{-1}. Although Riley et al. did not measure UV intensity in their test room, as explained in Appendix 2, we estimated average UV intensity in the upper-room zone to be 30 $\mu W/cm^2$ on the first test day, and 41 $\mu W/cm^2$ on the second and third test days. Therefore, on test day one, k_2 should have been 5.6 min^{-1} [(.0031 $cm^2/\mu W$-sec)(30 $\mu W/cm^2$)(60 sec/min)]; in comparison, Table II shows the model-derived k_2 value is 1.3 min^{-1} (for an air speed of 3 m/min), which differs by 4.3-fold. On test days two and three, k_2 should have been 7.6 min^{-1} [(.0031 $cm^2/\mu W$-sec)(41 $\mu W/cm^2$)(60 sec/min)]; Table II shows the model-derived k_2 values are 0.8 and 1.9 min^{-1} (for an air speed of 3 m/min), which differ by 9.5-fold and 4-fold, respectively. In summary, the k_2 values derived from the multi-zone models and test room data are less than, but within an order of magnitude of, the k_2 values predicted from the laboratory data. Given the uncertainties in modeling room geometries and air flows, and in estimating average UV intensity in the upper-room zone, we believe the two sets of k_2 values agree reasonably well.

CONCLUSIONS AND RECOMMENDATIONS

Figure 3 and Equations 11–13 indicate that a room can be poorly mixed, yet the slopes of the semi-log concentration decay curves at different points in the room can be close in magnitude. Moreover, the estimated slope of the observed semi-log decay curve cannot properly be converted to an equivalent ACH value at the measurement location unless room air is known to be well-mixed.[23] Note that the preceding analysis does not prove that on the first test day the concentration decay in the test room adhered to a three-zone model as described by Equations 11–13, or that the relative steady-state concentrations varied among three zones as described in Table I. Rather, the analysis demonstrates that Equations 11–13 are consistent with the reported data (other than the value of the initial room concentration), in which case the inference that upper room air UVGI added 10 Eq ACH throughout the test room is not established by these same data. Analogous statements apply to the reported Eq ACH values on the other two test days. In general, the interpretation of concentration decay data depends on the specific model for room air mixing that one assumes is appropriate; the decay data *per se* do not validate a particular model.

The preceding analysis has two implications for testing the efficacy of upper-room air UVGI, and of other control devices such as in-room air filtration units, in reducing viable *M. tb* concentrations. First, the test should be based on the steady-state

concentrations with and without the control device in operation, and should not be based on inferences drawn from the slopes of concentration decay curves. The measured steady-state concentrations are direct observations and do not require inferences based on a particular model of room air mixing. Second, steady-state concentrations should be measured at different points of interest in a room, including in the near field of the contaminant source. These different measurements directly assess the degree of air mixing in the room and the magnitude of the near-field effect. An example of these kinds of measurements are the efficacy tests conducted by Miller-Leiden and colleagues of in-room filtration units and dilution ventilation.[29]

ACKNOWLEDGMENTS

Dr. Nicas was supported by NIOSH/CDC Award No. K01-OH00155-01. Dr. Miller was supported by the Chancellor's Postdoctoral Fellowship at the University of Colorado, Boulder. The ideas expressed are solely the authors' and do not necessarily represent the official views of the funding agencies.

REFERENCES

1. Fineberg, H.F.; Wilson, M.E.: Social Vulnerability and Death by Infection. N Engl J Med 334(13):859–869 (1996).
2. Lopez, A.D.: Causes of Death in Industrial and Developing Countries: Estimates for 1985–1990. In: *Disease Control Priorities in Developing Countries*, Oxford University Press, Washington DC (1993).
3. Bloom, B.R.; Murray, C.J.L.: Tuberculosis: Commentary on a Reemergent Killer. Science 257:1055–1064 (1992).
4. Dooley, S.W.; Jarvis, W.R.; Snider, D.E.: Mycobacterium tuberculosis. In: *Hospital Epidemiology and Infection Control*, pp. 1200–1223. Williams & Wilkins, Baltimore (1996).
5. Jarvis, W.R.: Nosocomial Transmission of Multidrug-Resistant *Mycobacterium tuberculosis*. Research in Microbiologie 144:117–122 (1993).
6. Frankel, D.H.: Tuberculosis Falling in LA. Lancet 345:1565 (1995).
7. Frieden, T.R.; Fujiwara, P.I.; Washko, R.M.; et al.: Tuberculosis in New York City-Turning the Tide. N Engl J Med 333:229–233 (1995).
8. Riley, R.L.; O'Grady, F.: Airborne Infection: Transmission and Control. MacMillan Company, New York (1961).
9. American Thoracic Society/Centers for Disease Control: Diagnostic Standards and Classification of Tuberculosis. Am Rev Resp Dis 142:725–735 (1990).
10. Centers for Disease Control and Prevention: Guidelines for Preventing the Transmission of *Mycobacterium tuberculosis* in Health-Care Facilities. Mortality and Morbidity Weekly Report 43(RR-13):1–132 (1994).
11. Frieden, T.R.: Tuberculosis Control and Social Change. Am J Pub Health 84:1721–1723 (1994).
12. Monno, L.; Angarano, G.; Carbonara, S.; et al.: Emergence of Drug-Resistant *Mycobacterium tuberculosis* in HIV-Infected Patients. Letter to the Editor. Lancet 337(8745):852 (1991).
13. American Society of Heating, Refrigerating and Air-Conditioning Engineers: 1991 ASHRAE Handbook: Heating, Ventilating, and Air-Conditioning Applications. American Society of Heating, Refrigerating and Air-Conditioning Engineers, Atlanta (1991).
14. Nagin, D.; Pavelchak, N.; London, M.; et al.: Control of Tuberculosis in the Workplace: Engineering Controls. Occup Med: State of the Art Rev 9:609–630 (1994).
15. Summer, W.: Ultraviolet and Infrared Engineering, p. 197. Interscience Publishers, Inc., New York (1962).
16. Wells, W.F.: Airborne Contagion and Air Hygiene. Harvard University Press, Cambridge, MA (1955).
17. Riley, R.L.; Knight, M.; Middlebrook, G.: Ultraviolet Susceptibility of BCG and Virulent Tubercle Bacilli. Am Rev Resp Dis 113:413–418 (1976).
18. Macher, J.M.; Alevantis, L.E.; Chang, Y.-L.; et al.: Effect of Ultraviolet Germicidal Lamps on Airborne Microorganisms in an Outpatient Waiting Room. Appl Occup Environ Hyg 7(8):505–513 (1992).
19. Macher, J.M.; Alevantis, L.E.; Chang, Y.-L.; et al.: Letter to the Editor. Appl Occup Environ Hyg 9(7):462 (1994).
20. Stead, W. W.; Yeung, C.; Hartnett, C.: Probable Role of Ultraviolet Irradiation in Preventing Transmission of Tuberculosis: A Case Study. Infect Control Hosp Epidemiol 17(1):11–13 (1996).
21. Riley, R.L.; Permutt, S.: Room Air Disinfection by Ultraviolet Irradiation of Upper Air: Air Mixing and Germicidal Effectiveness. Arch Environ Health 22:208–219 (1971).
22. Nardell, E.A.: Interrupting Transmission from Patients with Unsuspected Tuberculosis: A Unique Role for Upper-Room Ultraviolet Air Disinfection. Am J Infect Control 23:156–164 (1995).
23. Nicas, M.: Estimating Exposure Intensity in an Imperfectly Mixed Room. Am Ind Hyg Assoc J 57:542–550 (1996).
24. Furtaw, E.J.; Panadian, M.D.; Nelson, D.R.; et al.: Modeling Indoor Air Concentrations Near Emission Sources in Imperfectly Mixed Rooms. J Air & Waste Manage Assoc 46:861–868 (1996).
25. Heinsohn, P.: Tuberculosis Resource Guide. CR-106146. Electric Power Research Institute, Palo Alto (1996).
26. Hopewell, P.: Factors Influencing the Transmission and Infectivity of *Mycobacterium tuberculosis*: Implications for Clinical and Public Health Management. In: Respiratory Infections, pp. 191–216. Churchill Livingstone, New York (1986).
27. Matthews, T.G.; Thompson, C.V.; Wilson, D.L.; et al.: Air Velocities Inside Domestic Environments: An Important Parameter in the Study of Indoor Air Quality and Climate. Environ Int 15:545–550 (1989).
28. Sandberg, M.: What Is Ventilation Efficiency? Build Environ 16:121–135 (1981).
29. Miller-Leiden, S.; Lobascio, C.; Nazaroff, W.W.; et al.: Effectiveness of In-Room Air Filtration and Dilution Ventilation for Tuberculosis Infection Control. J Air & Waste Manage Assoc 46:869–882 (1996).

APPENDIX 1

General Solutions for the Three-Zone Model Equations

Consider the set of differential equations defined by Equations 6–8 in the main text. By adding the trivial expression $dG/dt = 0$, the system of four equations can be written in the matrix form as follows:

$$\begin{bmatrix} C'_U(t) \\ C'_L(t) \\ C'_{NF}(t) \\ G'(t) \end{bmatrix} = \begin{bmatrix} -a & b & 0 & 0 \\ c & -d & e & 0 \\ 0 & f & -g & h \\ 0 & 0 & 0 & 0 \end{bmatrix} \times \begin{bmatrix} C_U(t) \\ C_L(t) \\ C_{NF}(t) \\ G \end{bmatrix} \quad [A1]$$

$$\text{where: } a = \frac{[(k_1 + k_2) \cdot V_U + \beta_1]}{V_U}, \quad b = \frac{\beta_1}{V_U}, \quad c = \frac{\beta_1}{V_L}$$

$$d = \frac{(k_1 \cdot V_L + \beta_1 + \beta_2 + Q)}{V_L}, \quad e = \frac{\beta_2}{V_L}, \quad f = \frac{\beta_2}{V_{NF}}$$

$$g = \frac{(k_1 \cdot V_{NF} + \beta_2)}{V_{NF}}, \quad h = \frac{1}{V_{NF}}$$

For convenience, the 4×4 coefficient matrix on the right-hand side of Equation A1 is denoted **A**. The general solutions to these equations are of the form:

$$\begin{bmatrix} C_U(t) \\ C_L(t) \\ C_{NF}(t) \\ G \end{bmatrix} = \alpha_1 \cdot e^{\lambda_1 \cdot t} \cdot \mathbf{X_1} + \alpha_2 \cdot e^{\lambda_2 \cdot t} \cdot \mathbf{X_2} + \alpha_3 \cdot e^{\lambda_3 \cdot t} \cdot \mathbf{X_3} + \alpha_4 \cdot e^{\lambda_4 \cdot t} \cdot \mathbf{X_4} \qquad [A2]$$

where λ_1 through λ_4 are the eigenvalues of matrix **A**, $\mathbf{X_1}$ through $\mathbf{X_4}$ are the corresponding 4×1 eigenvectors, and α_1 through α_4 are scalar coefficients that depend on the concentrations in the three zones at some reference time, say, $t = 0$. Note that Equation A2 applies only if the four eigenvalues are real, distinct numbers.

The eigenvalues and eigenvectors of matrix **A** can be found by standard linear algebra techniques. One eigenvalue will be $\lambda = 0$, which is denoted here as λ_4. For realistic room scenarios, the remaining eigenvalues λ_1, λ_2, and λ_3 will be unique negative numbers. By convention, let $|\lambda_1| < |\lambda_2| < |\lambda_3|$. The expression for these parameters are as follows:

$$\lambda_1 = -2\sqrt{\frac{(a + d + g)^2 - 3(ad + ag - bc + dg - ef)}{9}} \times \cos\left(\frac{\theta + 2\pi}{3}\right) - \frac{a + d + g}{3}$$

$$\lambda_2 = -2\sqrt{\frac{(a + d + g)^2 - 3(ad + ag - bc + dg - ef)}{9}} \times \cos\left(\frac{\theta + 4\pi}{3}\right) - \frac{a + d + g}{3}$$

$$\lambda_3 = -2\sqrt{\frac{(a + d + g)^2 - 3(ad + ag - bc + dg - ef)}{9}} \times \cos\left(\frac{\theta}{3}\right) - \frac{a + d + g}{3}$$

where:

$$\theta = \cos^{-1}\left(\frac{[2(a + d + g)^3 - 9(a + d + g)(ad + ag - bc + dg - ef) + 27(adg - aef - bcg)]/54}{\sqrt{\left(\frac{(a + d + g)^2 - 3(ad + ag - bc + dg - ef)}{9}\right)^3}}\right)$$

When the corresponding eigenvectors are determined and substituted into Equation A2, the matrix expression becomes the following set of four equations:

$$C_U(t) = \alpha_1 \cdot e^{\lambda_1 \cdot t} + \alpha_2 \cdot e^{\lambda_2 \cdot t} + \alpha_3 \cdot e^{\lambda_3 \cdot t} + \alpha_4 \qquad [A3]$$

$$C_L(t) = \alpha_1 \cdot \frac{\lambda_1 + a}{b} \cdot e^{\lambda_1 \cdot t} + \alpha_2 \cdot \frac{\lambda_2 + a}{b} \cdot e^{\lambda_2 \cdot t} + \alpha_3 \cdot \frac{\lambda_3 + a}{b} \cdot e^{\lambda_3 \cdot t} + \alpha_4 \cdot \frac{a}{b} \qquad [A4]$$

$$C_{NF}(t) = \alpha_1 \cdot \frac{f(\lambda_1 + a)}{b(\lambda_1 + g)} \cdot e^{\lambda_1 \cdot t} + \alpha_2 \cdot \frac{f(\lambda_2 + a)}{b(\lambda_2 + g)} \cdot e^{\lambda_2 \cdot t} + \alpha_3 \cdot \frac{f(\lambda_3 + a)}{b(\lambda_3 + g)} \cdot e^{\lambda_3 \cdot t} + \alpha_4 \cdot \frac{ad - bc}{be} \qquad [A5]$$

$$G = \alpha_4 \cdot \frac{adg - aef - bcg}{beh} \qquad [A6]$$

The coefficient α_4 is completely specified by Equation A6. If $G = 0$, $\alpha_4 = 0$. If $G > 0$, $\alpha_4 = [beh/(adg - aef - bcg)]G$. The expressions for α_1, α_2, and α_3 depend on specifying a set of initial value conditions, for example, $C_{NF}(0)$, $C_L(0)$, and $C_U(0)$. However, the expressions are cumbersome and are not presented here. By comparing Equations 3–5 in the main text with Equations A3–A5, it can be seen that:

$$\omega_1 = \alpha_1, \quad \omega_2 = \alpha_2, \quad \omega_3 = \alpha_3, \quad \omega_4 = \alpha_4$$

$$\omega_5 = \alpha_1 \cdot \frac{(\lambda_1 + a)}{b}, \quad \omega_6 = \alpha_2 \cdot \frac{(\lambda_2 + a)}{b},$$

$$\omega_7 = \alpha_3 \cdot \frac{(\lambda_3 + a)}{b}, \quad \omega_8 = \alpha_4 \cdot \frac{a}{b}$$

$$\omega_9 = \alpha_1 \cdot \frac{f(\lambda_1 + a)}{b(\lambda_1 + g)}, \quad \omega_{10} = \alpha_2 \cdot \frac{f(\lambda_2 + a)}{b(\lambda_2 + g)},$$

$$\omega_{11} = \alpha_3 \cdot \frac{f(\lambda_3 + a)}{b(\lambda_3 + g)}, \quad \omega_{12} = \alpha_4 \cdot \frac{ad - bc}{be}$$

APPENDIX 2

Point Source Summation Calculations of UV Intensity

The point source summation (PSS) method[1] was used to calculated the light intensity distribution within the *M. bovis* test room. In this method the UV lamp is approximated as a series of co-linear point sources of radiation. The total intensity

at any point in the room is computed by adding the contribution of each point source:

$$I(r, Z_0) = \sum_{n=1}^{N} \frac{S/N}{4\pi (r^2 + Z_n^2)} \qquad [A7]$$

where: I is intensity ($\mu W/cm^2$); r is radial distance from the UV lamp (cm); Z_0 is distance along the width axis of the room which we assumed was parallel to the lamp (cm); N is the total number of individual lamp elements (note: the number of divisions is arbitrary); S is the total lamp power available (μW); $Z_n = Z_0 - [(L \times n)/N]$, for $n = 1, 2, \ldots, N$ (cm); and L is the lamp arc length (cm). For the *M. bovis* test room experiments, we assumed the lamp length was L = 76.2 cm, and we divided the lamp into N = 76 elements.

Equation A7 assumes complete transmittance of UV irradiation through air. Although the effects of dissipation and absorbance are accounted for in this model, reflection and refraction are not included. Ignoring reflection is a reasonable assumption because UV irradiation is not reflected efficiently by most surfaces. For example, laboratory measurements of the fraction of 254 nm radiation reflected by different types of surfaces showed that the least reflecting was unpainted wood at 3.2 percent, and the most reflecting was stainless steel at 19.5 percent.[2] Another possible source of error in Equation A7 is the estimate of the lamp power, which strongly depends on surface temperature and lamp age.[3] Reported power values are only accurate for the specific set of conditions under which they were measured.

In the present application, the irradiated upper zone was divided into many different two-dimensional planes radiating outward from the lamp to the room walls (Figures 5 and 6). The vertical height of the irradiated upper zone corresponds to that reported in the Riley et al. paper: 0.61 m for the first test day and

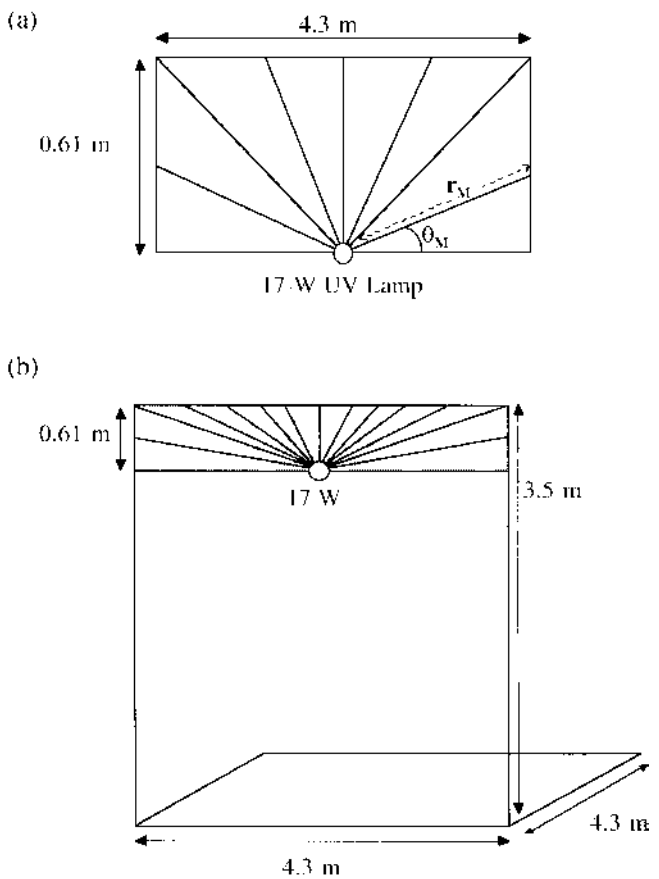

FIGURE 5

(*a*) A side view of the upper-room zone irradiated by the 17-W lamp on test day 1. The M^{th} radial line originating at the UV lamp represents a plane of length r_M and width 430 cm. The M^{th} radial plane was conceptually rotated through an angle θ_M to form a sector of a circle. (*b*) A three-dimensional view of the room (not drawn to scale) with only the 17-W lamp operating, which is the configuration pertaining to test day 1.

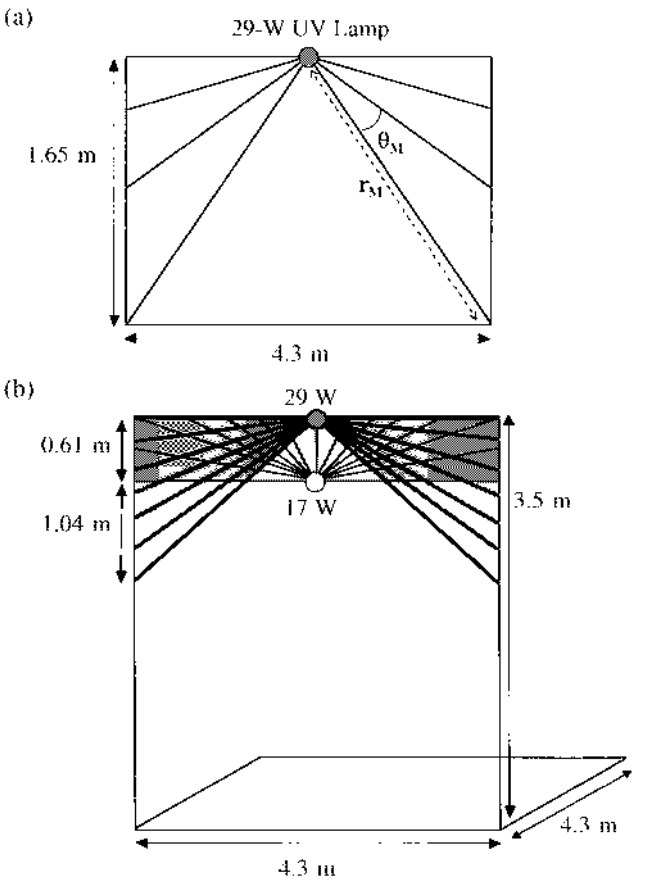

FIGURE 6

(*a*) A side view of the upper-room zone irradiated by the 29-W lamp on test days 2 and 3. The M^{th} radial line originating at the UV lamp represents a plane of length r_M and width 430 cm. The M^{th} radial plane was conceptually rotated through an angle θ_M to form a sector of a circle. (*b*) A three-dimensional view of the room (not drawn to scale) with both the 17-W and 29-W lamps operating, which is the configuration pertaining to test days 2 and 3.

1.65 m for the second and third test days. The floor dimensions of the test room were 5.8 m × 3.4 m; however, because it was not clear how the UV lamp was oriented, we assumed a square room configuration (4.3 m × 4.3 m) with the same floor area, 18.4 m^2. Thus, the width of each radial plane equals the assumed width of the upper zone, 4.3 m (14 ft). The length of each radial plane, r, equals the radial distance from the lamp to the wall. $I(r, Z_0)$ was calculated at 1-cm increments within each radial plane.

Note that on test day 1, the 17-W lamp was suspended 0.61 m down from the ceiling and baffled to prevent irradiation below the horizontal but permit irradiation through a 180° arc above the horizontal. Therefore, the entire upper zone cross-sectional area shown in Figure 5 was irradiated. On test days 2 and 3, a 29-W lamp was operated in addition to the 17-W lamp. The 29-W lamp was mounted to the ceiling and baffled in a manner to permit irradiation toward the room walls but not below 1.65 m from the ceiling. Therefore, only the outer wedges (the two right triangles) of the upper zone cross-sectional area shown in Figure 6 were irradiated by this lamp.

To obtain the average UV intensity in the irradiated upper zone, a volume-weighted average intensity was computed as follows:

$$\bar{I} = \sum_{h=1}^{M} \left[\sum_{i=1}^{r_h} \frac{w(h, i)}{A} \left(\sum_{j=1}^{430} \frac{I(h, i, j)}{430} \right) \right] \qquad [A8]$$

$$w(h, i) = \frac{(\theta_h) i^2}{2} - \frac{(\theta_h)(i-1)^2}{2}, \quad \text{for } i = 1, \ldots, r_h \qquad [A9]$$

$$A = \sum_{h=1}^{M} \sum_{i=1}^{r_h} w(h, i) \qquad [A10]$$

where M is the number of radial planes comprising the upper zone volume, r_h is the length (cm) of the h^{th} radial plane ($h = 1, \ldots, M$) extending from the lamp to the wall, and θ_h is the angle (radians) through which the h^{th} radial plane is conceptually rotated to form a sector of a circle. The quantity A is the sum of the sector areas associated with the M radial planes. The number of planes was chosen such that A was within 3 percent of the irradiated cross-sectional area. For the 17-W lamp on day 1, we used 24 planes which yielded A = 2.65 m^2, compared to an irradiated cross-sectional area of 2.62 m^2 (0.61 m × 4.3 m) for this day. For the 29-W lamp on days 2 and 3, we used 16 planes which yielded A = 3.45 m^2, compared to an irradiated cross-sectional area of 3.54 m^2 for these two days; the latter area corresponds to the outer wedges (the two right triangles) in Figure 6.

To explain the logic of Equation A8 briefly, for each radial distance i out from the lamp along the h^{th} radial plane, UV intensities at 430 points (1 cm apart) across the width of the plane were calculated according to Equation A7. These 430 intensities were averaged, as represented by the summation term indexed by j in Equation A8. This "width-average" UV intensity was assigned to an area w(h, i) computed by Equation A9. The quantity w(h, i) is the area of a sector bound by the h^{th} radial plane, a radial plane separated by angle θ_h, an arc of radial distance i out from the lamp, and an arc of radial distance $i - 1$ out from the lamp. In turn, the area w(h, i) was weighted by the total irradiated area A. Summing the products of the respective width-average UV intensities and sector area weights across all radial distances within a plane and all radial planes yielded the average UV intensity $\bar{I}$ in the irradiated portion of the upper zone. Because width-average UV intensities were used, $\bar{I}$ is inherently a volume-weighted average.

For test day 1, the reported lamp power was 17 W and the assumed upper zone vertical height was 0.61 m. However, all lamp power is not output as UV-C, and we assumed that only 30 percent of the lamp power was output as UV-C,[4] or S = 0.3 × 17 W = 5.1 W. This resulted in an estimated average intensity of 30 $\mu W/cm^2$ in the irradiated upper zone on test day 1.

For test days 2 and 3, a 29-W lamp was operated in addition to the 17-W lamp, and the upper zone vertical height was 1.65 m. The average intensity in this upper zone due to the 17-W lamp was 11 $\mu W/cm^2$, which is the product of 30 $\mu W/cm^2$ (estimated for test day 1) and the fraction 0.37 of the upper zone volume irradiated by the 17-W lamp on test days 2 and 3. That is, the upper zone cross-sectional area on days 2 and 3 was 7.1 m^2 (1.65 m × 4.3 m), but the 17-W lamp irradiated only 2.62 m^2 of this area (0.61 m × 4.3 m).

For the second lamp with reported power of 29 W, we assumed that = 0.3 × 29 W = 8.7 W. This resulted in an estimated average intensity of 30 $\mu W/cm^2$ in the upper zone on test days 2 and 3 due to the second lamp; this estimate accounts for the partial irradiation of the upper zone due to this lamp (see Figure 6). By assuming that the intensities due to the 17-W and 29-W lamps were additive, the estimated average intensity in the upper zone on test days 2 and 3 due to both lamps was 41 $\mu W/cm^2$.

The highest intensities occur nearest to the lamp, and the intensity decreases proportional to $1/r$ away from the lamp. To illustrate, for the 17-W lamp (assuming 70 percent lamp power attenuation), the estimated intensity 1 cm away from the lamp's center was 16,500 $\mu W/cm^2$, whereas the intensity 61 cm away from the lamp's center was 97 $\mu W/cm^2$. Due to incomplete air mixing within a typical room, many airborne bacteria may never reach the areas of highest intensity nearest the lamp. A better understanding of room air flow is needed to determine the fraction of bacteria exposed to levels of UV irradiation needed to inactivate them.[2] One approach to investigating the actual UV exposure of airborne bacteria is computational fluid dynamics modeling. The latter can account for indoor air and particle movement, and can provide more detailed information on flow field and particle concentration distributions.[5,6]

REFERENCES

1. Jacob, S.M.; Dranoff, J.S.: Light Intensity Profiles in a Perfectly Mixed Photoreactor. AIChE J 16(3):359–363 (1970).
2. Blatchley, III, E.R.: Numerical Modeling of UV Intensity: Application to Collimated-Beam Reactors and Continuous-Flow Systems. Wat Res 31(9):2205–2218 (1997).

3. Environmental Protection Agency. Design Manual: Municipal Wastewater Disinfection. EPA/625/1-86/021. EPA, Water Engineering Research Laboratory, Cincinnati, OH (1986).
4. Nardell, E.A.: Interrupting Transmission from Patients with Unsuspected Tuberculosis: A Unique Role for Upper-Room Ultraviolet Air Disinfection. Am J Infect Control 23:156–164 (1995).
5. Chen, Q.; Jiang, Z.; Moser, A.: Control of Airborne Particle Concentration and Draught Risk in an Operating Room. Indoor Air 2:154–167 (1992).
6. Chow, W.K.; Fung, W.Y.: Numerical Studies on the Indoor Air Flow in the Occupied Zone of Ventilated and Air-Conditioned Space. Build Environ 31(4):319–344 (1996).